Available online at www.sciencedirect.com

jmr&t Journal of Materials Research and Technology

www.jmrt.com.br

Original Article

Short-term creep properties of Ti-6Al-4V alloy subjected to surface plasma carburizing process

Verônica Mara Cortez Alves de Oliveira[a,*], *Mariane Capellari Leite da Silva*[a], *Cátia Gisele Pinto*[a], *Paulo Atsushi Suzuki*[a], *João Paulo Barros Machado*[b], *Vanessa Motta Chad*[c], *Miguel Justino Ribeiro Barboza*[a]

[a] *Escola de Engenharia de Lorena, Universidade de São Paulo, Lorena, SP, Brazil*

[b] *Instituto Nacional de Pesquisas Espaciais (INPE), São José dos Campos, SP, Brazil*

[c] *Instituto de Ciências Agrárias e Tecnológicas, Universidade Federal do Mato Grosso, Rondonópolis, MT, Brazil*

ARTICLE INFO

Article history:
Received 30 October 2014
Accepted 28 May 2015
Available online 3 July 2015

Keywords:
Short-term creep
Ti-6Al-4V
Plasma carburizing

ABSTRACT

The aim of this study was to investigate the short-time creep behavior of Ti-6Al-4V by plasma carburizing, which was performed at 725 °C for 6 h in a 50% Ar – 45% H_2 – 5% CH_4 gas mixture. Nano and microhardness testing, optical microscopy, TEM, X-ray diffraction and optical profilometry were used to characterize the samples. Furthermore, short-term creep tests were performed under a constant tensile load in air at 600 °C using a dead-weight-creep-rupture machine. The carburizing treatment resulted in a compound layer measuring approximately 1.7 μm in thickness with a hardness of 815 HV and a composition of $TiC_{0.66}$. The creep properties of the "Widmanstätten + carburized" specimens were improved relative to those of untreated specimens. TEM and fracture analysis indicated creep deformation process attributed mainly to α phase deformation and fracture by intergranular decohesion.

1. Introduction

Titanium alloys are widely used in the automotive, biomedical, aeronautic and other industries. These alloys exhibit special physical, mechanical and chemical characteristics that justify their use instead of other less costly materials [1,2]. At the same time, these alloys are not properly suitable for mechanical engineering applications that require good tribological properties and low reactivity [3]. Because of this limitation, many studies have been conducted with the aim of increasing the corrosion and creep properties of titanium alloys when exposed to high temperature [4].

Superficial thermochemical treatments have been applied to improve the mechanical strength, abrasion resistance and corrosion resistance of these materials, particularly at high temperatures [4,5]. Amongst the methods available today, plasma surface modification represents a very interesting technique. This method is based on the diffusion of an interstitial element on a material's surface using a plasma. The most common plasma treatments used are nitriding, carburizing and nitrocarburizing. Compared with the nitriding process,

* *Corresponding author.*
E-mail: veronicamcaoliveira@gmail.com (V.M.C.A. de Oliveira).

http://dx.doi.org/10.1016/j.jmrt.2015.05.006

carburizing is more difficult and less frequently used because titanium cannot solubilize carbon so easily [6]. In fact, the behavior of titanium alloys modified by plasma carburizing and the effect of this treatment on the mechanical properties of these materials are not well known [7–10]. The entire creep life of a titanium component could reach up to 120,000 h, what makes creep measurements more difficult [11]. Therefore, this study aims to evaluate the effects of plasma carburizing on Ti-6Al-4V alloy subjected to creep conditions at 600 °C, in order to ensure failure in a short time (short-term creep test). The short-term creep test method is widely used by many authors, who perform preliminary studies on creep behavior of Ti-6Al-4V alloy for structural applications [12–16].

2. Experimental

In this study, annealed Ti-6Al-4V alloy was used. Widmanstätten morphology was obtained by holding samples at 1050 °C for 30 min, followed by furnace cooling (6 °C/min) until 700 °C and air cooling until room temperature (*Widmanstätten* condition). Plasma carburizing was performed using an MP 400 equipment with DC-pulsed source and 30 kW at 725 °C for 6 h in an atmosphere composed of 50% Ar – 45% H_2 – 5% CH_4 ("Widmanstätten + carburized" condition). The surface morphology of the specimens, etched using Kroll's solution, was analyzed using optical microscopy. The carburized layer and the microstructure of crept samples were observed by scanning electron microscopy (SEM). The hardness of the specimens was measured using a Berkovich nanoidentor in the transversal section (initiating at outermost surface), with a load of 5 mN for 30 s. XRD analysis was carried out at room temperature with a CuKα radiation source, using a graphite filter, over the range of $20° < 2\theta < 95°$ in steps of 0.05° and a counting time of 1 s. Optical profilometry was used to determine the average roughness (Ra) of the samples surfaces; measurements were taken in the VSI (vertical scanning interferometry) mode. Creep tests were carried out using cylindrical creep specimens with 39 mm gauge length and 6 mm diameter, on an *Instron Model M3 Creep and Stress Rupture Tester* with 30 kN capacity under constant load in the range from 222 to 300 MPa at 600 °C. The dislocation structures of the specimens were observed by TEM.

3. Results

3.1. *Microstructural characterization*

Fig. 1(a) and (b) shows the cross-section of an α + β Widmanstätten microstructure under both conditions: *Widmanstätten* and "Widmanstätten + carburized". The carburized layer showed an average thickness of 1.7 μm. The average Vickers microhardness values for the *Widmanstätten cross-section sample* and carburized layer correspond to 334 ± 18 (HV) and 815 ± 61 (HV), respectively. Fig. 2 shows the evolution of nanohardness as function of depth (μm). The diffusion zone of carbon reached about 10 μm. The nanohardness values of carburized layer are in the same order of magnitude of the values obtained from the microhardness test. The nanohardness value tends to decrease toward the substrate.

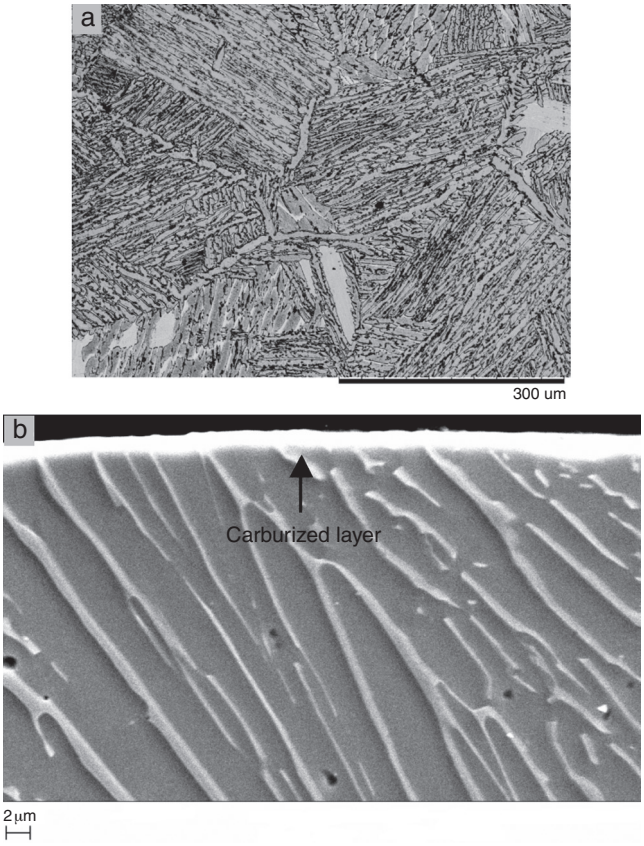

Fig. 1 – SEM images of Ti-6Al-4V alloy microstructure: (a) Widmanstätten and (b) "Widmanstätten + carburized".

Fig. 3 shows XRD patterns of "Widmanstätten + carburized" Ti-6Al-4V alloy. The phases α (HCP), β (BCC) and the carbide TiC (FCC) were identified.

Table 1 compares the phase lattice parameters, calculated by XRD analysis compared with those reported in the literature [17].

The α and β phases presented lattice parameters inferior to those reported in the literature for titanium (Ti). The

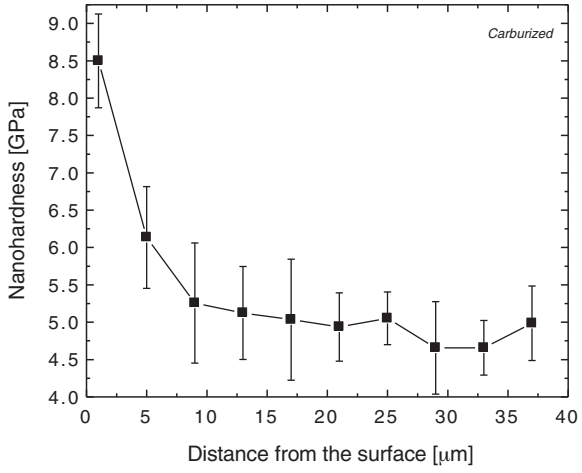

Fig. 2 – Hardness of "Widmanstätten + carburized" Ti-6Al-4V alloy against the distance from surface.

Table 1 – Calculated lattice parameters of the studied phases.

Phases	Lattice parameters [10^{-10} m]	Carburized sample	Literature [17]	Crystal lattice
α Ti	*a*	2.92	2.95	HC
	c	4.68	4.68	
β Ti	*a*	3.25	3.31	BCC
TiC	*a*	4.29	4.326	FCC

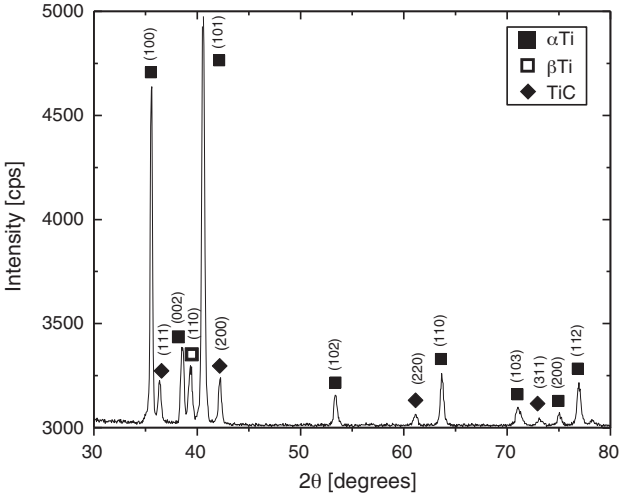

Fig. 3 – XRD patterns of "Widmanstätten + carburized" Ti-6Al-4V alloy.

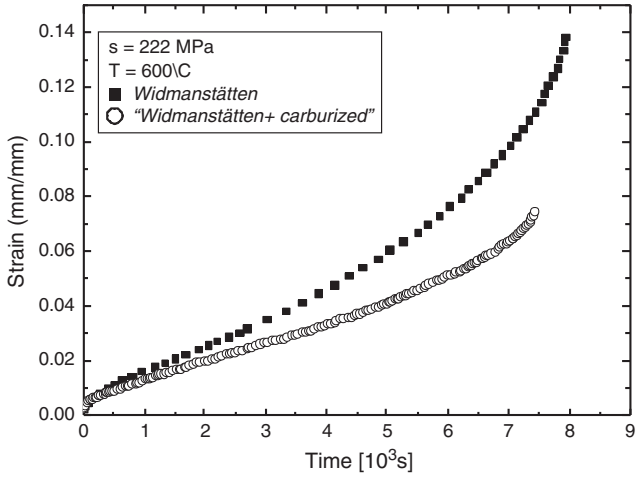

Fig. 4 – Creep curve of Widmasntätten and "Widmanstätten + carburized" samples, at 600 °C and 222 MPa.

alloying elements aluminum (Al) and vanadium (V), which have atomic radii smaller than the radius of titanium, replace titanium in the crystal lattice, thus reducing the lattice parameters [18]. The TiC carbide tended to form non-stoichiometric compounds with composition ranging from $TiC_{0.55}$ to $TiC_{0.95}$, which produced lattice parameters ranging from 4.2832 to 4.3172 Å [19]. Liu and Dupont have assumed that this parameter varies linearly with the carbon content of the carbide [20]. Using the same assumption, in this study, the carbide formed in the carburized layer might have the chemical formula $TiC_{0.66}$.

The carburized layer presented an increase in average roughness of 57% (Ra = 2.02 μm) when compared to the *Widmanstätten* sample (Ra = 1.29 μm). The greater average roughness indicates the irregularity of the carburized layer (TiC) and may contribute to the presence of stress concentrators on the layer's surface.

3.2. *Creep tests*

Fig. 4 displays representative creep curves of deformation (ε) *versus* time (t) at 600 °C and 222 MPa for the *Widmanstätten* and "Widmanstätten + carburized" condition.

Table 2 shows the main creep experimental parameters obtained at 600 °C for the *Widmanstätten* and "Widmanstätten + carburized" specimens.

In general, the deformation ε_0 tends to increase as a function of the applied stress. Due to the hardening induced by carbon diffusion, the "Widmanstätten + carburized" alloy shows lower values of instantaneous deformation (ε_0). The steady-state creep rate $\dot{\varepsilon}_S$ increases with the applied stress for both conditions studied. Relative to those of the *Widmanstätten* alloy, the steady-state creep rate values of the "Widmanstätten + carburized" alloy are 12–38% inferior.

Fig. 5 shows the dependence of the steady-state creep rate (5a) and time to fracture (5b) on the applied stress.

Eq. [1] describes the dependence of the steady-state creep rate on stress and temperature [21].

$$\dot{\varepsilon}_S = B\sigma^n \exp\left(-\frac{Q}{RT}\right) \quad (1)$$

where Q is the activation energy for creep in the secondary region, *B* a constant that depends on the microstructure, temperature and applied stress (σ), *n* the stress exponent, *R* the gas constant and *T* absolute temperature. The combination of Q and *n* values indicates the main creep mechanism that controls a given deformation process [21]. The slopes of the plot $Ln\dot{\varepsilon}_S \times Ln\sigma$, which is presented in Fig. 5(a), provide an estimate of *n*.

The values of $n = 6.70$ for the *Widmanstätten* alloy and $n = 5.64$ for the "Widmanstätten + carburized" alloy are in accordance with results of Barboza et al. [4,22] and Reis et al. [23,24], who studied Ti-6Al-4V in air and in a nitrogen atmosphere. These authors obtained *n* values between 4.25 and 6.46. Furthermore, Chen et al. [25] and Luo et al. [11], who studied Ti-60 and Titanium 834, respectively, obtained *n* values between 4.7 and 6.4.

The behavior of the time to fracture as a function of the applied stress is shown in Fig. 5(b). It decreases with increasing stress. At 222 MPa, the times to fracture of the *Widmanstätten* and "Widmanstätten + carburized" alloys are similar. At

Table 2 – Creep experimental parameters obtained at 600 °C for *Widmanstätten* and "Widmanstätten + carburized" specimens.

Parameters	"Widmanstätten + Carburized"				*Widmanstätten*		
	222 MPa	250 MPa	278 MPa	300 MPa	222 MPa	250 MPa	300 MPa
ε_0 [mm/mm]	0.0022	0.00302	0.00421	0.0043	0.00238	0.00331	0.00626
$\dot{\varepsilon}_S$ [1/s]	6.961×10^{-6}	1.352×10^{-5}	2.125×10^{-5}	4.069×10^{-5}	8.991×10^{-6}	1.540×10^{-5}	6.544×10^{-5}
t_f [10^3 s]	7.451	3.014	1.665	1.221	7.938	3.891	0.816
ε_f [mm/mm]	0.0746	0.0774	0.0503	0.0739	0.138	0.107	0.093

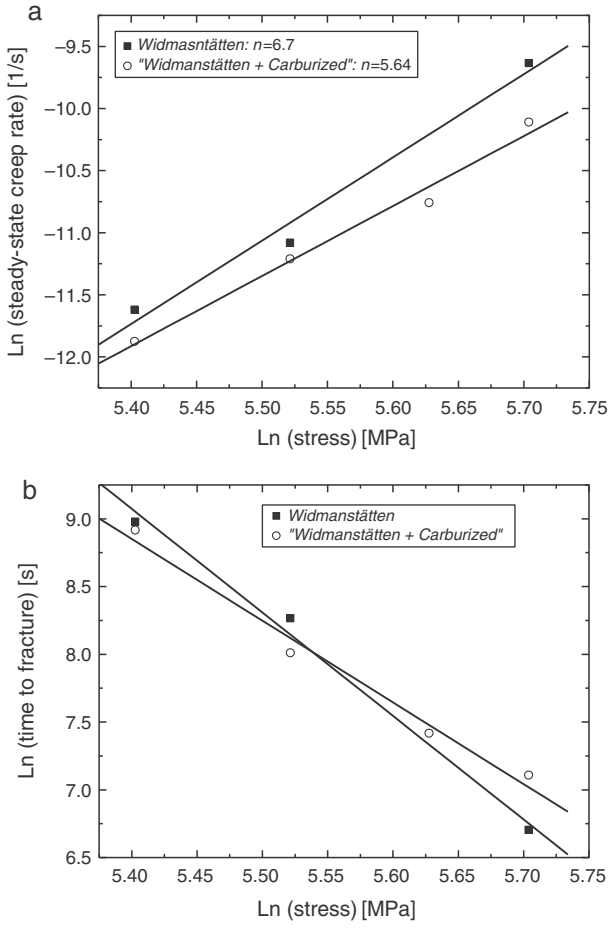

Fig. 5 – (a) Dependence of steady-state rate on applied stress at 600 °C for the Widmanstätten and "Widmanstätten + carburized" specimens (the slope is *n*). (b) Dependence of time to fracture on applied stress at 600 °C for the *Widmanstätten* and "Widmanstätten + carburized" specimens.

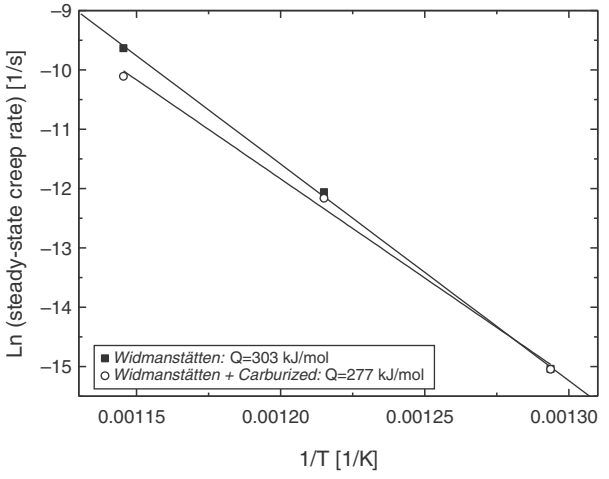

Fig. 6 – Dependence of steady-state rate on temperature for *Widmanstätten* and "Widmanstätten + carburized" specimens at 300 MPa (the slope is −Q/R).

Table 3 – Dependence of steady-state rate on temperature for *Widmanstätten* and "Widmanstätten + carburized" specimens at 300 MPa.

Temperature [°C]	Steady-state creep rate ($\dot{\varepsilon}_S$ [1/s])	
	Widmanstätten	"Widmanstätten + Carburized"
500	2.936×10^{-7}	2.915×10^{-7}
550	5.770×10^{-6}	5.220×10^{-6}
600	6.544×10^{-5}	4.069×10^{-5}

250 MPa, the lifetime of the "Widmanstätten + carburized" specimen decreased approximately 29% relative to that of the *Widmanstätten* specimen. However, at 300 MPa, the time to fracture increased 1.5 times under the "Widmanstätten + carburized" condition. The unsteady behavior of the time to fracture can be related to the increasing average roughness induced by plasma carburizing, which made the specimen surface less uniform. The increase in resistance indicated by the lower steady-state creep rates and the embrittlement indicated by the decrease in the final deformation (ε_f) could be associated with the hard layer of TiC introduced in the material which promotes more stress concentration and solid solution hardening due to the diffusion of carbon in α phase.

The dependence of the steady-state creep rate on temperature at 300 MPa is presented in Fig. 6 and Table 3.

The increase in temperature made the carburizing process more effective because the difference between the steady-state creep rates, under each condition, increase with temperature (Table 3). Fig. 6 illustrates this behavior. The percentage difference between the steady-state creep rates of the *Widmanstätten* and "Widmanstätten + carburized" specimens at 300 MPa are 0.7% at 500 °C, 9.5% at 550 °C and 37.8% at 600 °C. The carburized layer behaves as a barrier against the oxygen diffusion, which is a thermally activated phenomenon (the higher the temperature, the greater atoms transport activity). Thus, the carburized layer is more effective (compared with Widmanstätten condition) at higher temperatures where

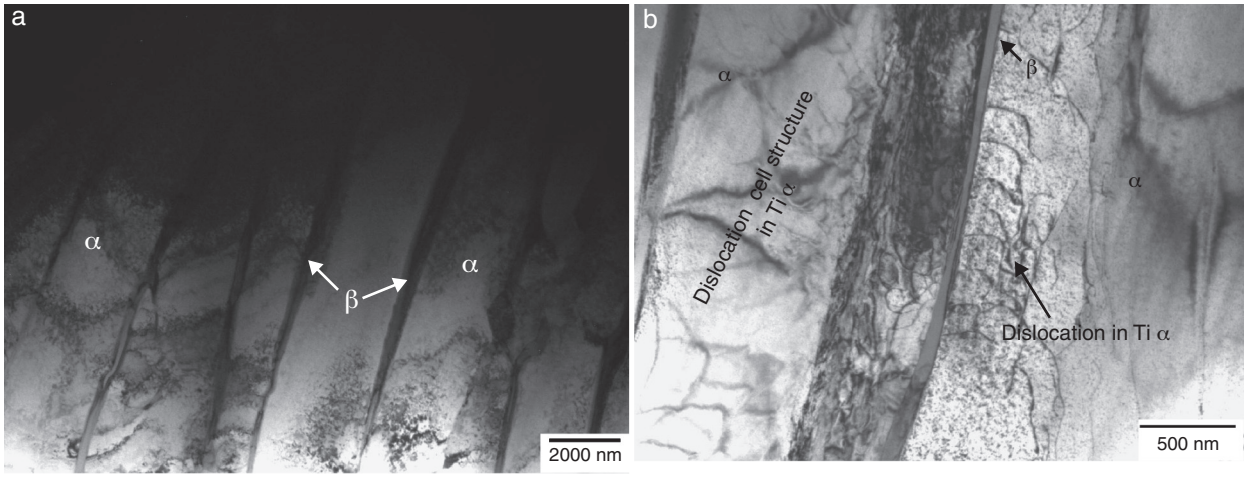

Fig. 7 – TEM micrographs of the dislocation substructures present in crept specimens at 600 °C: (a) *Widmanstätten* condition, 222 MPa; (b) "Widmanstätten + carburized" condition, 300 MPa.

the oxidation effect is more destructive because of the higher oxygen diffusion toward Ti-6Al-4V alloy.

The apparent activation creep energy was determined by calculating the steady-state creep rate at 500, 550 and 600 °C at 300 MPa for the *Widmanstätten* and "Widmanstätten + carburized" specimens (Fig. 6). The values Q = 303 kJ/mol for the *Widmanstätten* alloy and Q = 277 kJ/mol for the "Widmanstätten + carburized" alloy are in agreement with the results of Tang et al. [26], Gollapudi et al. [27] and Chen et al. [25], who studied creep of titanium-based alloys. The analysis of the values of the activation energy and stress exponent at 600 °C suggests that the creep mechanism under both conditions is associated with dislocation climbing processes [12,13,22,27–29].

3.3. *Dislocation substructure analysis*

Fig. 7 shows TEM images of the crept samples deformed at 600 °C.

The micrographs of both specimens depict dislocation cell structures. Under both conditions, the β phase presents a lower dislocation density compared with the α phase. Therefore, the creep deformation process can be attributed mainly to α phase deformation, as reported by Warren et al. [30], Tsuji et al. [9] and Chen et al. [25].

3.4. *Fracture analysis*

Fig. 8 shows transversal and longitudinal sections of samples crept under both conditions.

Fig. 8(a)–(d) shows a typical alveolar structure (dimples) associated with intergranular decohesion. The intergranular fracture mode can be linked to grain size due to the low capability, under these conditions, to accommodate the deformation induced by creep [31]. Fig. 8(e) and (f) illustrates the coalescence of creep cavities generated at grain boundary and triple points (indicated by arrows), where microvoids nucleation is initiated [16,32]. The results of fractrographic analysis are in accordance with those reported by Park et al. [16].

The growth of cavities (fracture process) is controlled by the strain ahead of the cavity. This aspect is confirmed using the Monkman–Grant relationship (Eq. [2]), which shows the proportionality between time to fracture and steady-state creep rate:

$$\dot{\varepsilon}_S^k(t_f) = C_{MG} \tag{2}$$

where k and C_{MG} are the constants [32]. Fig. 9 shows the correlation of steady-state creep rate and rupture life expressed by Monkman–Grant relation.

In this case, were found to *Widmanstätten* condition, $k = 1.13$ and $C_{MG} = 0.0147$, and to "Widmanstätten + carburized" condition, $k = 1.04$ and $C_{MG} = 0.0273$. The data are distributed along two distinct straight lines with approximately the same k and different C_{MG}. The slight reduction in the value of k and the observed increase in C_{MG} can be associated with lower values of creep ductility of the alloy modified by plasma carburizing process.

3.5. *Surface treatment influence on microstructure and mechanical properties of Ti-6Al-4V alloy*

Surface treatments involving the diffusion of an interstitial element can modify the microstructure of Ti-6Al-4V alloy by introducing a larger amount of α-Ti phase formation, grain growth, a harder layer (called α case) formation and fine precipitates nucleation [33–35].

To examine the amount of α-Ti and grain growth during plasma carburizing, two cylindrical specimens were heat treated to simulate the time and temperature of the plasma carburizing treatment. The samples were analyzed using the ImageJ software (phase proportion), and grain size was measured according to the intercept method [18]. Analysis was made over 120 images with 50 and 100 times magnification for each condition studied (Widmanstätten and "Widmanstätten + carburized") and grain size analysis performed on 20 images of 50 times magnification for each condition studied.

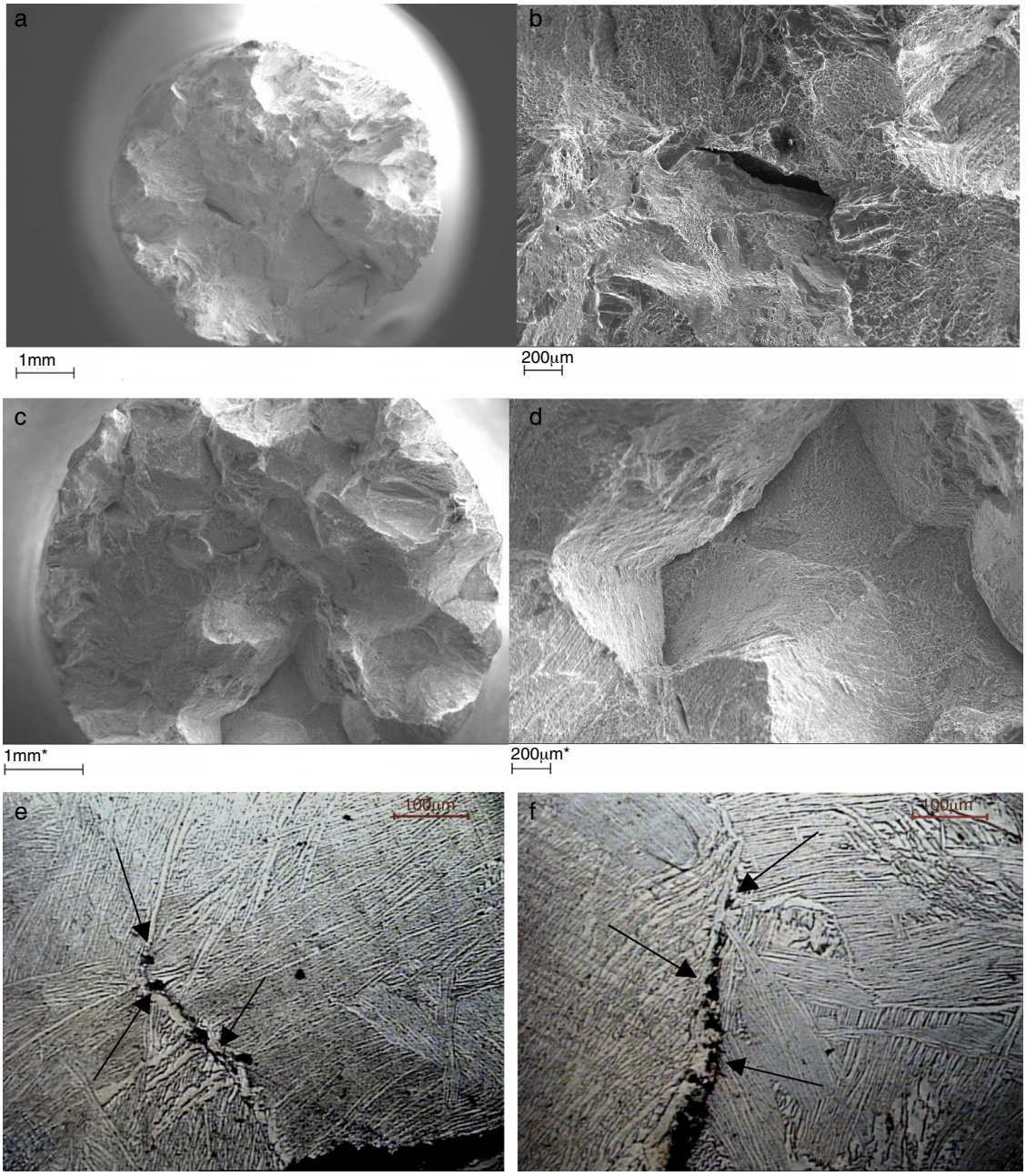

Fig. 8 – Fracture surface morphologies: SEM image of transversal section of (a, b) Widmanstätten Ti-6Al-4V at 600 °C and 300 MPa and (c, d) "Widmanstätten + carburized" Ti-6Al-4V at 600 °C and 222 MPa; optical image of longitudinal section of (e) *Widmanstätten* Ti-6Al-4V at 600 °C and 300 MPa; and (f) "Widmanstätten + carburized" Ti-6Al-4V at 600 °C and 222 MPa.

All data were statistically analyzed and are presented in Table 4.

Based on Table 4 and taking into account the errors, it can be considered that the surface treatment does not modify the relative amount of α-Ti phase, and grain size of Ti-6Al-4V alloy. In fact, the Widmanstätten morphology was purposely chosen to have a stable morphology at high temperatures, changing only with the annealing time (at temperatures above 980 °C)

Table 4 – Statistical analysis of the phase amount (%) and grain size (mm) change with plasma carburizing process.

Heat treatment	Amount of β phase – Ti (%)			Grain size (mm)		
	Average	Error	Median	Average	Error	Median
Widmanstätten	35.5	1.0	35.8	1.25	0.05	1.23
"Widmanstätten + carburized"	33.5	0.7	33.2	1.10	0.09	1.16

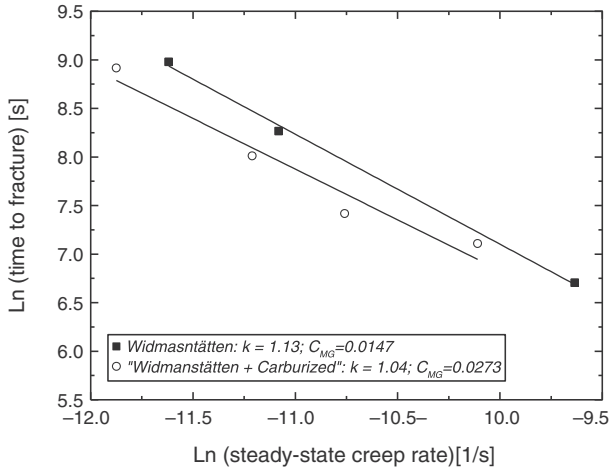

Fig. 9 – Relationship between time to fracture and steady-state creep rate according to Monkman–Grant equation.

and cooling rate [33]. The plasma carburizing treatment did not exceed 725 °C and did not involve any step where the cooling rate could alter the microstructure in some way.

The formation of the layer, known as α case, is very common in the oxidation process and thermochemical treatments where a α-Ti phase stabilizing element is involved (IIIA and IVA metals group and the interstitial elements C, N and O) [5,33]. Pitt and Ramulu [34] reported that the titanium alloy weight increasing when exposed to temperatures around 650 °C is due to the oxygen diffusion, which forms a diffusion zone known as α case. This region is described as a hard and brittle region [34]. The α case thickness measurement was made by nanohardness analysis. Thus, observing the microhardness profile (Fig. 2), it can be concluded that the surface treatment resulted in a combination composed of TiC hard layer and a solid solution-hardened region. The carbon element reached about 9 μm depth in Ti-6Al-4V alloy, resulting in the formation of α case. Therefore, it is correct to conclude that the creep improvement behavior observed in the present work is due to a combination of hard ceramic layer, which has high thermal stability, plus the solid solution-hardened α case layer. However, Ti-6Al-4V alloy suffers with oxidation effects at 600 °C and the simple stabilization of α-Ti phase on surface would not be effective for improving the creep properties of Ti-6Al-4V alloy.

When the Ti-6Al-4V alloy is aged between 500 and 600 °C, precipitation in the microstructure occurs of a phase known as α_2 (with the formula Ti_3Al) due to aluminum presence which modifies the α-Ti phase field in a Ti-Al system [35–37]. Therefore, treatments that involve high temperatures and long times may result in the precipitation of this compound homogeneously and with nanometric dimensions. Ti_3Al improves titanium's mechanical properties, since this compound acts as a barrier to dislocation gliding. However, studies reported in the literature, where Ti_3Al was precipitated in a matrix of titanium, involved aging methods with rather large time ranging from 168 to 200 h of treatment, and the formed compound could be identified by XRD techniques [35–37]. The heat treatment time reported in the present study reached a maximum of 7 h and XRD analysis did not indicate the presence of this phase. Thus, Ti_3Al precipitation was not taken into account.

Finally, it can be concluded that surface treatments influence creep performance of Ti-6Al-4V alloy and is correlated with the ceramics surface protecting effect, which is harder and thermally stable. Any other microstructural modification seems to act secondarily on the mechanical properties of this alloy.

4. Concluding remarks

All specimens showed an α + β Widmanstätten microstructure. A carburized layer, 1.7 μm in width, is formed by $TiC_{0.66}$. Plasma carburizing increased the hardness value (815 HV) and average roughness (2.02 μm) of the specimens compared to the values measured for the *Widmanstätten* (1.29 μm and 334 HV) specimens. The short-term creep behavior improved with plasma carburizing, resulting in reduced instantaneous deformation and steady-state creep rates. However, the influence of plasma carburizing on the time to fracture was not clear and could be attributed to the increase in surface roughness observed. Based on the correlation between the activation energy and stress exponent values, it can be concluded that the creep mechanisms are associated with dislocation climbing creep processes, in the present creep conditions. TEM and fracture analyses of the *Widmanstätten* and "Widmanstätten + carburized" specimens indicate creep deformation process attributed mainly to α phase deformation and fracture by intergranular decohesion, respectively. Additionally, the steady-state creep rate and the rupture time are related by the Monkman–Grant relation with *k* about 1. The alloy modified by plasma carburizing exhibits a larger value of C_{MG}, which is associated with lower ductility. Therefore, the good mechanical properties of "Widmanstätten + carburized" Ti-6Al-4V justify the interest in better understanding the effects of plasma carburizing process to improve the performance of titanium alloys used in high-temperature applications. The present results involve very short creep durations and more creep tests should be carried out involving longer rupture times (of the order of hundreds or thousands hours), at other stress/temperature conditions, to confirm the creep properties mentioned in this work.

Conflicts of interest

The authors declare no conflicts of interest

Acknowledgements

The authors are grateful to FAPESP for financial support (Processes 2007/54987-0, 2008/52843-3, 2008/55782-5, 2009/51433-9, 2010/05367-1).

REFERENCES

[1] Leyens C, Peters M. Titanium and titanium alloys: fundamentals and applications. Weinheim: Wiley-VCH; 2003.

[2] Sagara M, Takayama I, Nishida T. Application of titanium for automotive use in Japan. Nippon steel technical report, vol. 62; 1994. p. 23–8.
[3] Zhecheva A, Sha W, Malinov S, Long A. Enhancing the microstructure and properties of titanium alloys through nitriding and other surface engineering methods. Surf Coat Technol 2005;200:2192–207.
[4] Barboza MJR, Moura Neto C, Silva CRM. Creep mechanisms and physical modeling for Ti-6Al-4V. Mater Sci Eng A 2004;369:201–9.
[5] Balazic M, Kopac J, Jackson MJ, Ahmed W. Review: Titanium and titanium alloy applications in medicine. Int J Nano Biomater 2003;1(1):3–34.
[6] Kim T, Park Y, Wey M. Characterization of Ti-6Al-4V alloy modified by plasma carburizing process. Mater Sci Eng A 2003;361:275–80.
[7] Tsuji N, Tanaka S, Takasugi T. Effects of combined plasma-carburizing and shot-peening on fatigue and wear properties of Ti-6Al-4V alloy. Surf Coat Technol 2009;203:1400–5.
[8] Tsuji N, Tanaka S, Takasugi T. Effect of combined plasma-carburizing and deep-rolling on notch fatigue property of Ti-6Al-4V alloy. Mater Sci Eng A 2009;499:482–8.
[9] Park YG, Wey MY, Hong SI. Enhanced wear and fatigue properties of Ti-6Al-4V alloy modified by plasma carburizing/CrN coating. J Mater Sci 2007;18:925–31.
[10] Luo Y, Ge S, Jin Z, Fisher J. Formation of titanium carbide coating with micro-porous structure. Appl Phys A 2010;98:765–8.
[11] Abdallah Z, Perkins K, Williams S. Advances in the Wilshire extrapolation technique – full creep curve representation for the aerospace alloy titanium 834. Mater Sci Eng A 2012;550:176–82.
[12] Boehlert CJ, Chen W. The elevated-temperature creep behavior of boron-modified Ti-6Al-4V alloys. Mater Trans 2009;50(7):1690–703.
[13] Ma ZY, Mishra RS, Tjong SC. High-temperature creep behavior of TiC particulate reinforced Ti-6Al-4V alloy composite. Acta Mater 2002;50:4293–302.
[14] Zhu SJ, Mukherji D, Chen W, Lu YX, Wang ZG, Wahi RP. Steady state creep behavior of TiC particulate reinforced Ti-6Al-4V composite. Mater Sci Eng A 1998;256:301–7.
[15] Park YG, Wey MY, Hong SI, Ikenaga M. Creep and high temperature fatigue resistance of Ti-6Al-4V modified by duplex plasma carburization/CrN coating. Solid State Phenom 2006;118:515–20.
[16] Seco FJ, Irisarri AM. Creep failure mechanisms of Ti-6Al-4V thick plate. Fatigue Fract Eng Mater Struct 2001;24:741–50.
[17] Villars P, Calvert I. Pearson's handbook of crystallographic data for intermetallic phases. Ohio: Materials Park; 1991.
[18] Callister WD Jr. Materials science and engineering: an introduction. New York: John Wiley & Sons; 2007.
[19] Capaldi MJ, Saidi A, Wood JV. Reaction synthesis of TiC and Fe-TiC composites. ISIJ Int 1997;37(2):188–93.
[20] Liu W, Dupont JN. Fabrication of functionally graded TiC/Ti composites by laser engineered net shaping. Scr Mater 2003;48:1337–42.
[21] Evans RW, Wilshire B. Introduction to creep. London: The Institute of Materials; 1993.
[22] Barboza MJR, Perez EAC, Medeiros MM, Reis DAP, Nono MCA, Piorino Neto F, et al. Creep behavior of Ti-6Al-4V and comparison with titanium matrix composites. Mater Sci Eng A 2006;428:319–26.
[23] Reis DAP, Silva CRM, Nono MCA, Barboza MJR, Piorino Neto J, Perez EAC. Effect of environment on the creep behavior of Ti-6Al-4V alloy. Mater Sci Eng A 2005;399:276–80.
[24] Reis AG, Reis DAP, Moura Neto C, Barboza MJR, Silva CRM, Piorino Neto F, et al. Influence of laser treatment on the creep of the Ti-6Al-4V alloy. Metall Mater Trans A 2011;42a:3031–4.
[25] Chen Z, Li J, Liu J, Wang Q, Liu J, Yang R. Creep behavior of fusion zone and base metal of the electron beam weldments of a near-alpha titanium alloy. J Mater Sci Technol 2010;26(6):564–71.
[26] Tang F, Nakazawa S, Hagiwara M. Transient creep of Ti-Al-Nb alloys. Mater Sci Eng A 2002;325:194–201.
[27] Gollapudi S, Charit I, Murty KL. Creep mechanisms in Ti-3Al-2.5V alloy tubing deformed under closed-end internal gas pressurization. Acta Mater 2008;56(10):2406–19.
[28] Ranganath S, Mishra RS. Steady state creep behaviour of particulate-reinforced titanium matrix composites. Acta Metall 1996;44(3):927–35.
[29] Hayes RW. Minimum strain rate and primary transient creep analysis of a fine structure orthorhombic titanium aluminide. Scr Mater 1996;34:1005–12.
[30] Warren J, Hsiung LM, Wadley HNG. High temperature deformation behavior of physical vapor deposited Ti-6Al-4V. Acta Metall 1995;43:2773–87.
[31] Brooks CR, Choudhury A. Metallurgical failure analysis. New York: McGraw-Hill; 1993.
[32] Kassner ME, Hayes TA. Creep cavitation in metals. Int J Plast 2003;19:1715–48.
[33] Donachie MJ Jr. Titanium: a technical guide. Ohio: ASM International; 1988.
[34] Pitt F, Ramulu M. Influence of grain size and microstructure on oxidation rates in titanium alloy Ti-6Al-4V under superplasticforming conditions. J Mater Eng Perform 2004;13(6):727–34.
[35] Lee D, Lee S, Lee Y. Effect of precipitates on damping capacity and mechanical properties of Ti-6Al-4V alloy. Mater Sci Eng A 2008;486:19–26.
[36] Lee K, Seo S, Lee K. Oxidation behaviors of TiAl(La)N coatings deposited by ion plating. Scr Mater 2005;52:445–8.
[37] Zhang SZ, Xu HZ, Li GP, Liu YY, Yang R. Effect of carbon and aging treatment on precipitation of ordered $\alpha 2$ in Ti-5.6Al-4.8Sn-2Zr-1Mo-0.35Si-0.7Nd alloy. Mater Sci Eng A 2005;408:290–6.